Thin Solid Films 519 (2011) 3032–3036

Contents lists available at ScienceDirect

Thin Solid Films

journal homepage: www.elsevier.com/locate/tsf

# Electrochromic properties of N-doped tungsten oxide thin films prepared by reactive DC-pulsed sputtering

Xilian Sun *, Zhimin Liu, Hongtao Cao

*Division of Functional Materials and Nano Devices, Ningbo Institute of Material Technology & Engineering, Chinese Academy Sciences, Ningbo, 315201, PR China*

ARTICLE INFO

*Article history:*
Received 10 January 2010
Received in revised form 30 November 2010
Accepted 7 December 2010

*Keywords:*
Tungsten oxide
Electrochromism
Structural properties
N-doping
DC-pulsed sputtering
Optical properties

ABSTRACT

In depositing nitrogen doped tungsten oxide thin films by using reactive DC-pulsed magnetron sputtering process, nitrous oxide gas ($N_2O$) was employed instead of nitrogen ($N_2$) as the nitrogen dopant source. The nitrogen doping effect on the structural and electrochromic properties of $WO_3$ thin films was investigated. **X-ray** diffraction (XRD) results show that the films are amorphous. Morphological images reveal that the films are characterized by a hybrid structure comprising nanoparticles embedded in amorphous matrix and open channels between the agglomerated nanoparticles, which promotes rapid charge transport through the film. Increasing the nitrogen doping concentration is found to decrease the nanoparticle size and the band gap energy. The electrochromic properties were studied using cyclic voltammetric and spectroeletrochemical techniques. The film with N content of ~5 at.% exhibits higher optical modulation and coloration efficiency as well as faster ion transport kinetics. The results reveal that electrochromic and lithium ion transport properties are moderately enhanced relative to the un-doped tungsten oxide thin films by appropriate content of dopant, due to the effects of nitrogen doping.



## 1. Introduction

Over the past years, tungsten oxide ($WO_3$) has been extensively studied due to its interesting physical and chemical properties. $WO_3$ shows a strong reversible field-aided ion intercalation behavior. Ions such as $Li^+$ can be easily introduced into the host $WO_3$ lattice. This ion insertion is combined with a strong change in the electronic and optical properties of the oxide, and this effect is exploited intensively in electrochromic devices, such as large area information displays, rear-view mirrors, smart windows for automobiles and energy saving architecture due to their low power consumption and high energy efficiency [1–3]. Amorphous $WO_3$ ($\alpha$-$WO_3$) has shown to be one of the excellent candidates for electrochromic applications [4,5]. When ions are intercalated, the charge-compensating electrons enter the localized states. The electronic structure of $WO_3$ is modified and this strongly alters the optical properties of the material from transparent to a deep blue color. Doping of metal ions in amorphous tungsten oxide has been investigated for the enhancement of their electrochromic, gas sensing and electrochemical properties [6–10]. Few reports have dealt with the electrochromic behavior of anion doping $\alpha$-$WO_3$. Recently, nitrogen doping of wide band gap transition metal oxide semiconductors has been studied to manipulate its chemical composition and thereby modifies its electronic and structural properties to use them in potential applications in nano-scale optoelectronic device [11–15].

Tungsten oxynitride is characterized by chemical inertness and good thermal stability, and it promises the possibility to tune the structural, optical and electrical properties in a wide range as desired for various applications [16–22]. As discussed early by Nakagawa [20] and Nanba [21], the changes in the bond overlap population of W–O bonds due to nitrogen doping cause lattice distortion, which localizes the electron at the tungsten site as described by small polaron absorption theory. This is also expected to play an influential role in improving electrochromic and lithium-insertion properties. Tungsten oxynitride thin films can be made either by dc reactive magnetron sputtering using metallic tungsten target in $N_2+O_2$ or $Ar+N_2+O_2$ atmosphere, or by pulsed laser deposition using ceramic $WO_3$ target in pure $N_2$ atmosphere[18,19,22]. However, detailed investigations of the films prepared by reactive DC-pulsed sputtering and the effects of nitrogen dopant in relation to the structure, morphology, electrochromic properties and lithium insertion properties are very limited. The reactive dc pulsed sputtering technique is able to eliminate the random arcing phenomena by supplying the dc power in the form of high negative pulses interrupted by small positive pulses. In this way the charge at the oxide surface on the target can be neutralized by attracting electrons during the positive part of the duty cycle. This technique can preserve high deposition rates compared to the RF techniques.

In this study, the reactive DC-pulsed sputtering was used to deposit undoped and N-doped tungsten oxide thin films. The nitrous oxide ($N_2O$) was used as the provider of N dopant source because of its easier ionization than nitrogen, hence enhancing the plasma density and deposition rate. The effect of $N_2O$ flow ratio on the structural and

* Corresponding author. Tel./fax: +86 0574 86685163.
*E-mail address:* xiliansun@163.com (X. Sun).

0040-6090/$ – see front matter © 2011 Elsevier B.V. All rights reserved.
doi:10.1016/j.tsf.2010.12.017

electrochromic properties of the N-doped tungsten oxide thin films was explored in this paper.

## 2. Experimental procedure

### 2.1. Sample preparation

Reactive DC-pulsed sputtering was utilized to prepare undoped and N-doped tungsten oxide thin films. High purity argon, oxygen and nitrous oxide gases were used as sputtering and reactive gases, respectively. The sputtering chamber was evacuated to $1.3\times10^{-4}$ Pa using a turbo molecular pump plus a dry pump before introducing the gases. Metallic tungsten target (2 inches in diameter and 99.99% in purity) was powered by a dc generator. The discharge was generated at a constant power of 120 W for dc polarization. The pulse frequency was 20 kHz, and the reverse time was 5 μs. Mass flow rates of Ar, $O_2$ and $N_2O$ were controlled by individual mass flow meter. For all studies, total gas flow and argon flow rate were kept at 28 sccm and 21 sccm, respectively. The flow rate ratio of oxygen and nitrous oxide ($N_2O$) was tuned systematically while maintaining the sum flow rate of oxygen and nitrous oxide at 7 sccm unchanged. In this paper, the $G$ value, defined as $G=N_2O/(N_2O+O_2)$, was used to monitor the nitrogen dopant. Before introducing the nitrous oxide or oxygen gas, the tungsten target was pre-sputtered for 10 min by Ar gas to remove the surface oxide layer and contaminations. Fused silica and fluorine tin oxide (FTO, 14 Ω/square) coated glass were used as substrates. Deposition was performed at room temperature to prevent crystallization of $WO_3$. Film thickness was controlled by deposition time.

### 2.2. Characterization

Film thickness was analyzed on Si substrate by a variable angle spectroscopic ellipsometer (J. A. Woollam, USA) in the range of 300–1500 nm. The crystallographic structure of the films was determined by X-ray diffraction (XRD) using a Bruker AXS D8 advance diffractometer with Cu $K_\alpha$ radiation. The spectral transmittance was measured at normal incidence using a Perkin-Elmer Lambda-980 spectrophotometer in the range of 300–2000 nm. Surface morphology was obtained by a field-emission scanning electron microscopy (FE-SEM, S-4800, HITACHI) operating at 8 kV equipped with an energy-dispersion spectrometer (EDS). EDS was employed for elemental analysis operating at 15 kV. The film surface topography was imaged using an atomic force microscope (AFM, Veeco Instruments, Dimension 3100 V) with a silicon nitride cantilever operated in tapping mode. The resulting AFM images were analyzed to estimate the film roughness. Electrochromic coloration and bleaching of the undoped and N-doped tungsten oxide thin films were performed in a conventional electrochemical cell: sputtered film as the working electrode, Pt foil as the counter electrode, Ag/AgCl as the reference electrode and 1 M $LiClO_4$/propylene carbonate solution as the electrolyte. The potential was swept from the natural electrode potential of the thin films to −0.6 V and then switched to +0.6 V using Model 273A (Princeton Applied Research) at a scan rate of 20 mV/s and 2 mV/s, respectively.

**Table 1**
Elemental composition, film thickness and surface roughness of tungsten oxide films with different $N_2O$ flow ratio.

| $G$ | Deposition rate (nm/min) | Film thickness (nm) | Amount of N incorporation (at.%) | RMS surface roughness (nm) | $E_g$ (eV) |
|---|---|---|---|---|---|
| 0 | 2.3 | 228 | – | 19.9 | 3.44 |
| 0.2 | 2.5 | 222 | 4.7 | 15.0 | 3.40 |
| 0.6 | 4.2 | 222 | 6.1 | 14.7 | 3.36 |
| 0.8 | 6.1 | 235 | 12.5 | 13.1 | 2.97 |

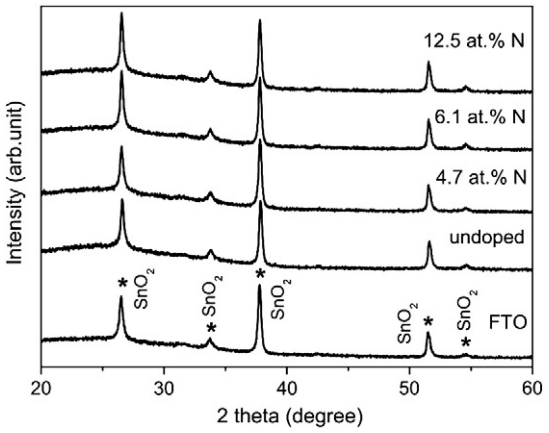


**Fig. 1.** XRD patterns of tungsten oxide thin films with various N concentrations. * denotes FTO peaks.

## 3. Results and discussion

### 3.1. Composition and structure

Film thicknesses of all the samples are found to be around 228 ± 7 nm and summarized in Table 1. The X-ray diffraction patterns for the films deposited at various $N_2O$ flow ratio on FTO coated glass substrates are illustrated in Fig. 1. It clearly shows that all the film patterns consist of a broad hump without discernable $WO_3$ diffraction peaks, except the superposed diffraction peaks of the FTO substrate. It indicates that the films are amorphous or mixed amorphous/nanocrystalline in nature. The diffraction patterns may result from the amorphous property or/and internal stress of tungsten oxide films, which is usually a feature of the films prepared by sputtering deposition at room temperature [23].

The compositional analysis of the tungsten oxide films prepared under various $N_2O$ flux is done using EDS spectra and the amount of nitrogen incorporated in the films is listed in Table 1. Fig. 2 depicts a typical EDS spectrum for the N-doped tungsten oxide film deposited at $G=0.8$. The analysis of the EDS spectra confirms the presence of N, O and W elements in the film. As seen from Table 1, the amount of nitrogen incorporated increases from ~5 at.% to ~13 at.% as $G$ increases from 0.2 to 0.8. The nitrogen content of these films did not linearly depend on $G$ because W ion possesses a stronger affinity to oxygen than to nitrogen. Thermodynamically, the formation of tungsten oxide is energetically favored over the formation of tungsten nitride layer: the standard Gibbs free energy of formation for $WO_3$ and $WO_2$ is −842.9 kJ/mol and −589.7 kJ/mol, respectively, which greatly exceeds the values for $W_2N$ (−22 kJ/mol) and WN (−15 kJ/mol) [22].

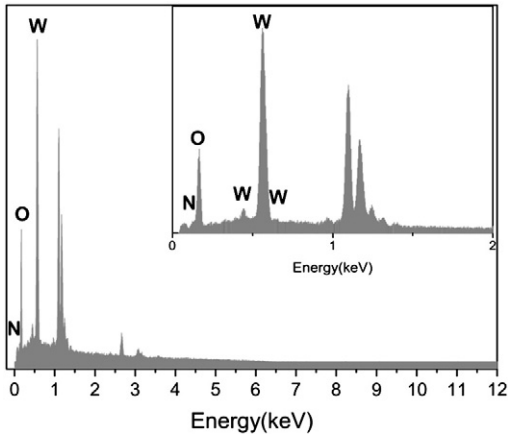


**Fig. 2.** EDS spectra of tungsten oxide thin films deposited at $G=0.6$.

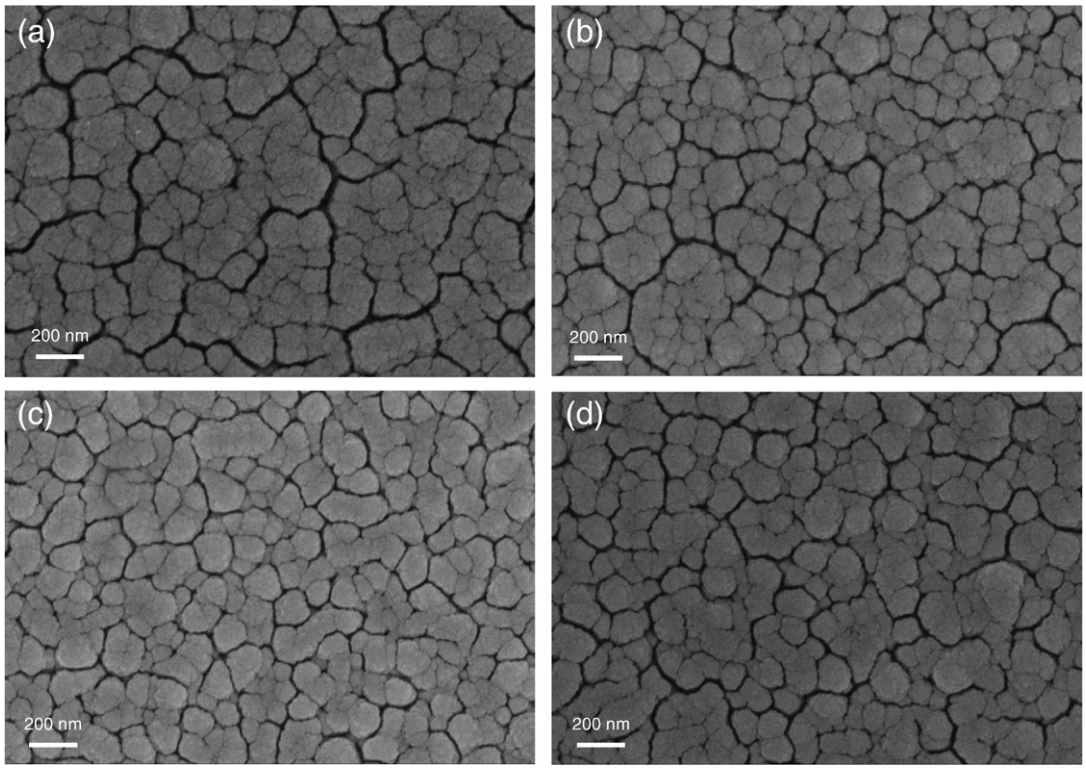


**Fig. 3.** Surface SEM micrographs of (a) undoped, (b) 4.7 at.%, (c) 6.1 at.% and (d) 12.5 at.% N-doped tungsten oxide thin films.

The structure and morphology for undoped and N-doped tungsten oxide thin films were examined using SEM and AFM. Fig. 3 displays the SEM micrographies of the samples. It can be seen that the film morphology consists of randomly distributed grains and pores between them. The enclosed observation of the film surface reveals that the grains are not homogeneous and looks like agglomerates or clusters with different nanosizes. And for N-doped tungsten oxide thin films, the grain size decreases due to nitrogen doping. On the other hand, it is also found that there are many channels along the inter-agglomerate boundaries. The higher proportion of channels and more porous surface of the film would facilitate intercalation of ions into the film and faster kinetics [24,25]. Moreover, the large surface roughness values of all the tungsten oxide films were calculated from AFM images of the surface (as shown in Table 1). Such structure increases the effective surface area, which results in a more resultful contact between the electrode and the electrolyte, thereby minimizing the ohmic drop across the cell. As a result, easier access of a large volume of ions into the film ensues in an amplification of the coloration efficiency [26].

### 3.2. Optical and electrochromic properties

The band gap energies ($E_g$) of the films are obtained from the absorption coefficient (α, calculated from the equation: $\alpha = 4k\pi/\lambda$,

**Table 2**
The electrochromic properties for undoped and N-doped $WO_3$ films.

| Amount of N incorporation (at.%) | Ion storage capacity ($mC/cm^2$) | $D_{in}$(1E-12) ($cm^2/s$) | *CE* at 633 nm ($cm^2/C$) |
|---|---|---|---|
| – | 15.7 | 3.4 | 38 |
| 4.7 | 20.1 | 10.4 | 42 |
| 6.1 | 17.0 | 3.9 | 29 |
| 12.5 | 16.4 | 3.2 | 20 |

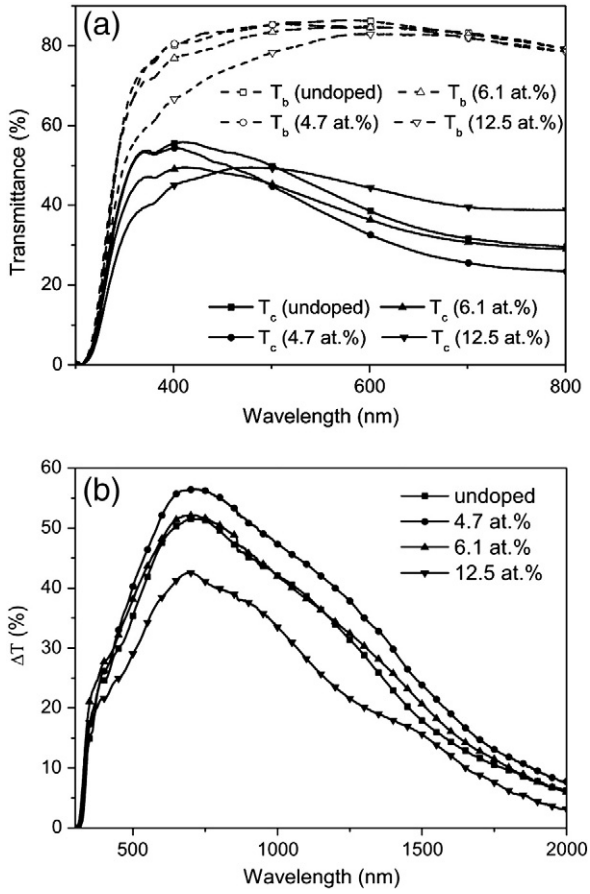


**Fig. 4.** Transmittance (a) and transmission modulation (b) of undoped, 4.7 at.%, 6.1 at.% and 12.5 at.% N-doped tungsten oxide thin films.

and the extinction coefficient k is evaluated from the spectroscopic ellipsometry analysis) using the relationship for indirect allowed transitions:

$$(\alpha h\nu)^{1/2} = A\left(h\nu - E_g\right). \quad (1)$$

where $A$, $h\nu$ and $E_g$ are a constant of proportionality, incident photon energy and optical band gap energy, respectively. The dependence of the band gap energy on different nitrous oxide flux is listed in Table 1. Compared with the undoped one, a systematic decrease in the band gap with nitrogen incorporation is observed for the films, resulting from a higher negative potential of the valence band of the N 2p orbital [20]. Futsuhara and Mohammed [26,27] have reported that the optical band gap energy is related to the difference in ionicity between metal-O and metal-N bonds. According to the Pauling theory, ionicity in single bonds enhances with increasing in the electro-negativity difference between two elements forming a single bond. The electro-negativity of oxygen (3.5) is larger than that of nitrogen (3.0), which indicates that the W–O bonds involve a larger charge transfer than the W–N bonds. Thus considering the coexistence of the W–O and W–N bonds in the films, the shift of the band gap to a lower energy can be attributed to both the decrease in ionicity and an increase in polarizability due to the formation of W–N bonds with increasing nitrogen concentration [28].

The films were colored and bleached with a constant current density of $-0.3$ mA/cm$^2$ for 120 s and $+0.3$ mA/cm$^2$ for 120 s in order to determine the transmission modulation and coloration efficiency, as listed in Table 2. Fig. 4 exhibits the transmittance and transmission modulation of undoped and N-doped tungsten oxide thin films with different N concentration. As can be seen from Fig. 4 (a), in the bleached state the transmittances of the films are ~80% in the visible spectrum. Upon $Li^+$ intercalation, the transmittances for these films fall down, with variations of 29–56%, 23–54%, 28–49.6% and 39–49.4% for $G=0$, 0.2, 0.6 and 0.8, respectively, which indicates neutral color with increasing N concentration in the $WO_3$ film. Then the transmittance modulations calculated from the transmittance differences between the colored and bleached states ($\Delta T = T_b - T_c$) are illustrated in Fig. 4(b). Compared to undoped tungsten oxide, N-doped tungsten oxide films yield much larger values in transmission modulation ($\Delta T$) except the sample at $G=0.8$ which is lower than that of the undoped one. The maximum $\Delta T$ at ~700 nm wavelength was 51.5%, 56.5%, 52%, and 42.3% for $G=0$, 0.2, 0.6 and 0.8, respectively. These findings are in line with the observation of a higher amount of ions being incorporated during the reactions. Coloration efficiencies ($CE(\lambda)$) can be estimated from the spectro-electrochemical data using the following relation:

$$CE(\lambda) = \Delta OD(\lambda)/(Q/A) = \log(T_b/T_c)/(Q/A) \quad (2)$$

where $T_b$ and $T_c$ are the transmittances of the film in the bleached and colored states, respectively. $Q$ is the amount of inserted charge. The $CE$ values for the undoped and N-doped $WO_3$ films as a function of N concentration are presented in Table 2. Clearly, it was observed that $CE$ values increases as N-doping concentration increases and found the maximum of 45 cm$^2$/C for the ~5 at.% N-doped samples and further increasing N concentration reduces the $CE$ values. This indicates that an appropriate number of nitrogen doping play a role in enhancing electrochromism.

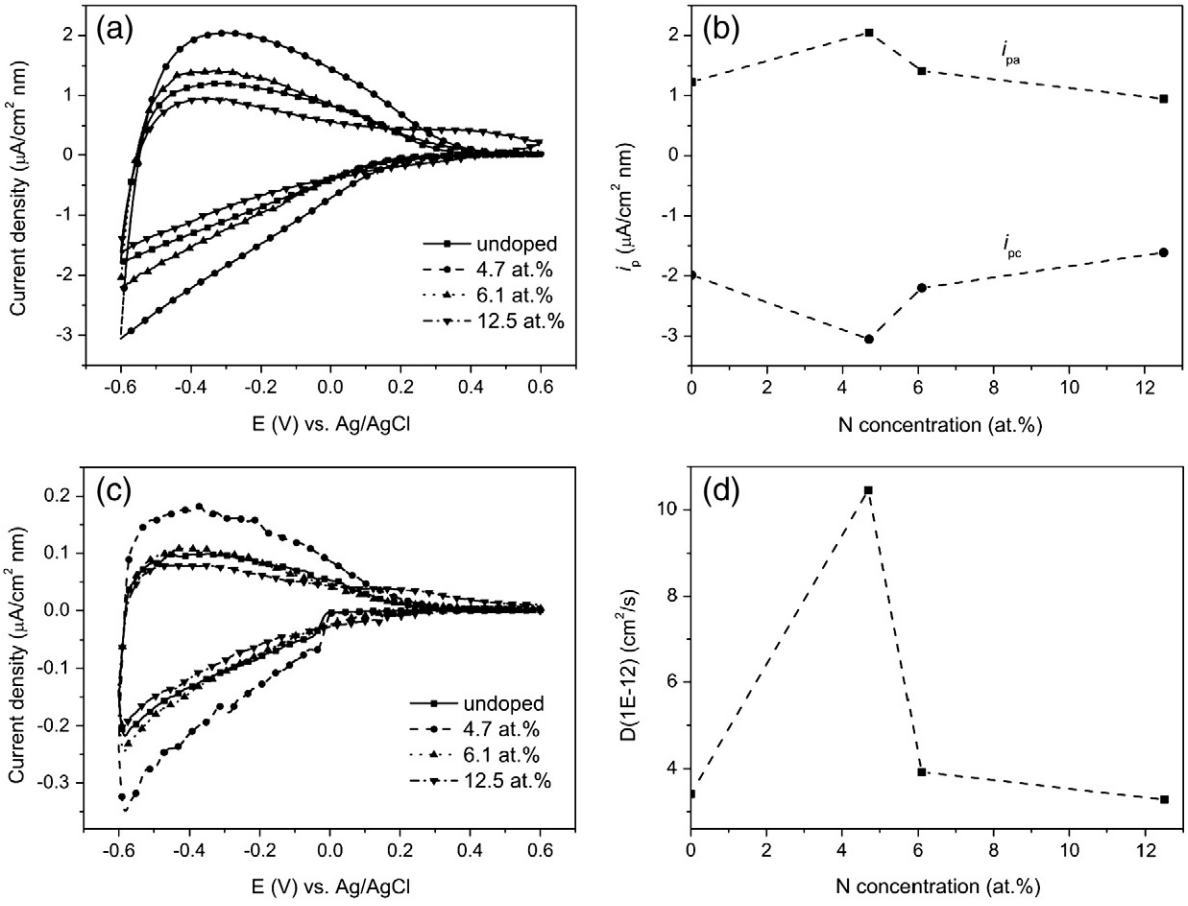


**Fig. 5.** (a) Cyclic voltammograms (20 mV/s), (b) peak current density ($i_{pa}$ and $i_{pc}$), (c) cyclic voltammograms (2 mV/s) and (d) diffusion coefficient ($D$) of undoped, 4.7 at.%, 6.1 at.% and 12.5 at.% N-doped tungsten oxide films.

Cyclic voltammograms (CV) were recorded for the undoped and N-doped samples with potential sweep between −0.6 and +0.6 V at a scan rate of 20 mV/s and shown in Fig. 5(a). All of the CVs were normalized to the geometric area of the electrode and to the thickness of tungsten oxide film, resulting in a unit of $\mu A\,cm^{-2}\,nm^{-1}$. The integrated cathodic-current density equates to the amount of lithium ions intercalated to form a tungsten bronze. The ion storage capacities of the films calculated from CV curves are summarized in Table 2. Compared with the cathodic charge quantities of undoped samples, the N-doped samples show a higher charge-insertion density over the same period of time, indicating faster kinetics. The cathodic and anodic peak current density ($i_{pc}$ and $i_{pa}$) data as a function of N concentration are shown in Fig. 5(b). It is observed that the cathodic and anodic current densities increased for ~5 at.% and ~6 at.% N-doped samples due to the ease of lithium ion diffusion into the films, whereas for ~13 at.% N-doped films, the cathode peak current density decreases as ions insertion in this film is low. This result is in line with the finding of ion diffusion coefficient (Fig. 5(d)). The shift of threshold voltage towards positive potential with increase in N concentration suggests that the structure offers an easy way to diffusion and charge transfer process of ions.

The effective diffusion coefficient $D$ for lithium ions can be estimated from the anodic peak current ($i_p$) dependence on the square root of the potential sweep rate ($v$) by assuming simple solid state diffusion controlled process [28]:

$$i_p = 2.72 \times 10^5 \times n^{3/2} \times D^{1/2} \times C_0 \times v^{1/2}. \quad (3)$$

where $i_p$ is the peak anodic current ($A\,cm^{-2}$), $n=1$ is the number of electrons involved in the process, $D$ ($cm^2 s^{-1}$) is the diffusion coefficient, $C_0$ is the solution concentration ($mol\,cm^{-3}$) and $v$ is the scan rate ($V\,s^{-1}$). It has been reported that diffusion coefficient deduced by CV peaks at low scan rates is credible, due to the quasi-equilibrium conditions in the case [29]. Therefore the diffusion coefficients at 2 mV/s scan rate are calculated and summarized in Table 2. It clearly shows that the diffusion coefficient increases as doping concentration increases up to ~6 at.%. However, the diffusion coefficient decreases for higher (~13 at.%) N-doped films. Noticeably, the charges inserted for all doped samples during intercalation process are always greater than the undoped one.

## 4. Conclusions

Nitrogen doping effects on the structural, compositional, morphological and electrochromic properties of tungsten oxide thin films deposited by reactive DC-pulsed sputtering technique have been investigated as a function of the amount of N incorporated in the $WO_3$ films. The band gap energy calculated from the absorption decreases with increasing N concentration. The size of nanoparticle decreases with nitrogen doping. Rapid lithium ion transport through the film is enabled through uniformly distributed nanosized channels and pores. Such nanosized channels between nanoparticles aid ion movement due to shorter diffusion path lengths. The effect can be manifested in ion diffusion coefficient that is found higher for the N-doped film than the undoped one.

## Acknowledgment

The authors gratefully acknowledge the financial support provided by Science and Technology Department of Zhejiang Province of China (2008C31G3220006).

## References

[1] G.A. Niklasson, C.G. Granqvist, J. Mater. Chem. 17 (2007) 127.
[2] S.K. Deb, Sol. Energy Mater. Sol. Cells 92 (2008) 245.
[3] C.G. Granqvist, G.A. Niklasson, A. Azens, Appl. Phys. A 89 (2007) 29.
[4] C.M. Lampert, Sol. Energy Mater. Sol. Cells 76 (2003) 489.
[5] E. Avendano, L. Berggren, G.A. Niklasson, C.G. Granqvist, A. Azens, Thin Solid Films 496 (2006) 30.
[6] S.R. Bathe, P.S. Patil, Solid State Ionics 179 (2008) 314.
[7] T. Brezesinski, D.F. Rohlfing, S. Sallard, M. Antonietti, B.M. Smarsly, Small 2 (2006) 1203.
[8] P.M.S. Monk, S.P. Akhtar, J. Boutevin, J.R. Duffield, Electrochim. Acta 46 (2001) 2091.
[9] C.O. Avellaneda, L.O.S. Bulhoes, Solid State Ionics 165 (2003) 117.
[10] A. Taurio, M. Catalano, R. Rella, P. Siciliano, W. Wlodarski, J. Appl. Phys. 93 (2003) 3816.
[11] X. Qiu, C. Burda, Chem. Phys. 339 (2007) 1.
[12] L. Lin, W. Lin, Y.X. Zhu, B.Y. Zhao, Y.C. Xie, Chem. Lett. 34 (2005) 642.
[13] S. Jeon, H. Kin, K. Yong, J. Vac. Sci. Technol. B 27 (2009) 671.
[14] B. Cole, B. Marsen, E. Miller, Y. Yan, B. To, K. Jones, M.A. Jassim, J. Phys. Chem. C 112 (2008) 5213.
[15] D. Paluselli, B. Marsen, E.L. Miller, R.E. Rocheleau, Electrochem. Solid-State Lett. 8 (2005) G301.
[16] T.E. Lucy, T.P.S. Clair, S.T. Oyama, J. Mater. Res. 13 (1998) 2321.
[17] Y.G. Shen, Y.W. Mai, J. Mater. Res. 15 (2000) 2437.
[18] N.M.G. Parreira, N.J.M. Carvalro, F. Vaz, A. Cavaleiro, Surf. Coat. Technol. 200 (2006) 6511.
[19] K.J. Lethy, S. Potdar, V.P.M. Pallai, V. Ganesan, J. Phys. D Appl. Phys. 42 (2009) 095412.
[20] K. Nakagawa, N. Miura, S. Matsumoto, R. Nakano, H. Matsumoto, Jpn. J. Appl. Phys. 47 (2008) 7230.
[21] T. Nanba, M. Ishikawa, Y. Sakai, Y. Miura, Thin Solid Films 445 (2003) 175.
[22] S.H. Mohamed, A. Anders, Surf. Coat. Technol. 201 (2006) 2977.
[23] X.G. Wang, Y.S. Jiang, N.H. Yang, L. Yuan, S.J. Pang, Appl. Surf. Sci. 143 (1999) 135.
[24] M. Deepa, A.K. Srivastava, K.N. Sood, S.A. Agnihotry, Nanotechnology 17 (2006) 2625.
[25] Y.S. Lin, Y.L. Chiang, J.Y. Lai, Solid State Ionics 180 (2009) 99.
[26] M. Futsuhara, K. Yoshioka, O. Takai, Thin Solid Films 317 (1998) 322.
[27] G. He, L.D. Zhang, G.H. Li, M. Liu, X.J. Wang, J. Phys. D Appl. Phys. 41 (2008) 045304.
[28] M. Deepa, R. Sharma, A. Basu, S.A. Agnihotry, Electrochim. Acta 50 (2005) 3545.
[29] G. Leftheriotis, S. Papaefthimiou, P. Yianoulis, Solid State Ionics 178 (2007) 259.